

NNLO QCD corrections for Drell–Yan p_T^Z and ϕ_η^* observables at the LHC

A. Gehrmann–De Ridder^{a,b}, T. Gehrmann^b, E.W.N. Glover^c, A. Huss^a, T.A. Morgan^c

^a*Institute for Theoretical Physics, ETH, CH-8093 Zürich, Switzerland*

^b*Department of Physics, University of Zürich, CH-8057 Zürich, Switzerland*

^c*Institute for Particle Physics Phenomenology, Department of Physics, University of Durham, Durham, DH1 3LE, UK*

E-mail: gehra@phys.ethz.ch, thomas.gehrmann@uzh.ch,
e.w.n.glover@durham.ac.uk, ahuss@phys.ethz.ch,
t.a.morgan@durham.ac.uk

ABSTRACT: Drell–Yan lepton pairs with finite transverse momentum are produced when the vector boson recoils against (multiple) parton emission(s), and is determined by QCD dynamics. At small transverse momentum, the fixed order predictions break down due to the emergence of large logarithmic contributions. This region can be studied via the p_T^Z distribution constructed from the energies of the leptons, or through the ϕ_η^* distribution that relies on the directions of the leptons. For sufficiently small transverse momentum, the ϕ_η^* observable can be measured experimentally with better resolution. We study the small p_T^Z and ϕ_η^* distributions up to next-to-next-to-leading order (NNLO) in perturbative QCD. We compute the ϕ_η^* distributions for the fully inclusive production of lepton pairs via Z/γ^* to NNLO and normalise them to the NNLO cross sections for inclusive Z/γ^* production. We compare our predictions with the ϕ_η^* distribution measured by the ATLAS collaboration during LHC operation at 8 TeV. We find that at moderate to large values of ϕ_η^* , the NNLO effects are positive and lead to a substantial improvement in the theory–data comparison compared to next-to-leading order (NLO). At small values of p_T^Z and ϕ_η^* , the known large logarithmic enhancements emerge through and we identify the region where resummation is needed. We find an approximate relationship between the values of p_T^Z and ϕ_η^* where the large logarithms emerge and find perturbative consistency between the two observables.

Contents

1	Introduction	1
2	Kinematics of the angular variable ϕ_η^* in the low-p_T^Z regime	4
3	Numerical results	5
3.1	Calculational setup	5
3.2	The transverse momentum distribution at low p_T^Z	6
3.3	The large ϕ_η^* region	7
3.4	The small ϕ_η^* region	10
4	Summary and conclusions	13

1 Introduction

The production of Z-bosons which subsequently decay into a pair of leptons is a Standard Model benchmark process at hadron colliders. It occurs with a large rate and, due to its clean final state signature, can be measured very accurately with small experimental uncertainties. It has been studied extensively at the LHC by the ATLAS [1, 2], CMS [3, 4] and LHCb [5] experiments.

When combined with precise theoretical predictions for related observables, there is the potential for accurate determinations of fundamental parameters of the theory. In particular, the transverse momentum distribution of the Z-boson has been one of the most studied observables. The high sensitivity of the p_T^Z spectrum to the distribution of gluons in the proton makes it a key observable for constraining parton distribution functions (PDF's).

For inclusive Z-production, restricting ourselves to the framework of QCD, corrections at next-to-next-to-leading order (NNLO) are available [6–9] and the present state of the art is obtained by combining the NNLO QCD corrections with a resummation of next-to-next-to-leading logarithmic effects (NNLL) [10]. This combination is necessary to predict the transverse momentum distribution of the Z-boson at small p_T^Z . In this region, large logarithmic corrections of the form $\ln^n(p_T^Z/m_{\ell\ell})$ appear at each order in the perturbative expansion in α_s , spoiling the convergence of the fixed-order predictions.

The transverse momentum of the Z-boson is caused by the emission of QCD radiation from the initial state partons. As a consequence, fixed order predictions at $\mathcal{O}(\alpha_s^2)$ in perturbative QCD, which are NNLO accurate for the inclusive cross section correspond only to NLO accurate predictions for the transverse momentum distributions. At high values of p_T^Z , namely above 20 GeV, both ATLAS and CMS observed a tension between the NLO predictions and their measurements of the p_T^Z distributions presented in the form of

fiducial cross sections for a restricted kinematical range of the final state leptons. Motivated by this observation, in a recent paper [11], we have used the parton-level event generator NNLOJET, as described in [12], to predict the Z-boson distributions at large transverse momentum to NNLO accuracy. We computed the fiducial cross section for the production of a Z-boson at finite transverse momentum fully inclusively on the hadronic final state. We found that when the p_T^Z distribution is normalised to the relevant di-lepton cross section, the NNLO predictions yield an excellent agreement with the measured distributions at $\sqrt{s} = 8$ TeV from both ATLAS and CMS over a large range of p_T^Z values above the selected cut of $p_T^Z = 20$ GeV. Given the importance of a precise determination of the p_T^Z spectrum for phenomenology, it is also crucial to have a thorough probe of the low p_T^Z domain as well. We therefore use the NNLOJET code to make predictions in the low transverse momentum region. As expected, the fixed order description will fail at sufficiently small p_T^Z , but it is also interesting to see exactly where this happens. In particular, we will show that the NNLO fixed order perturbative description extends to significantly lower p_T^Z than at NLO.

In the small p_T^Z region, the precision of direct measurements of the p_T^Z spectrum using the standard p_T^Z variable is limited by the experimental resolution on p_T^Z itself, and in particular on the resolution of the magnitude of the transverse momenta of the individual leptons entering p_T^Z . To probe the low p_T^Z domain of Z/γ^* production an alternative angular variable, ϕ_η^* , has been proposed [13] which minimises the impact of these experimental uncertainties. It is defined by

$$\phi_\eta^* \equiv \tan\left(\frac{\phi_{\text{acop}}}{2}\right) \cdot \sin(\theta_\eta^*). \quad (1.1)$$

In this definition, the acoplanarity angle is

$$\phi_{\text{acop}} \equiv \pi - \Delta\phi \equiv 2 \arctan\left(\sqrt{\frac{1 + \cos \Delta\phi}{1 - \cos \Delta\phi}}\right), \quad (1.2)$$

where $\Delta\phi$ is the azimuthal angle between the two leptons. The angle θ_η^* is the scattering angle of the leptons with respect to the proton beam direction in the reference frame that is boosted along the beam direction such that the two leptons are back-to-back in the (r, θ) plane. It is explicitly given by

$$\cos(\theta_\eta^*) \equiv \tanh\left(\frac{\eta^{\ell^-} - \eta^{\ell^+}}{2}\right), \quad (1.3)$$

where η^{ℓ^-} and η^{ℓ^+} are the pseudorapidities of the negatively and positively charged leptons respectively.

The variable ϕ_η^* measures the “deviation from back-to-backness” (acoplanarity) in the transverse plane and therefore vanishes at Born level where the azimuthal angle between the two leptons $\Delta\phi$ is exactly equal to π . Non-zero values of ϕ_η^* are produced by the same mechanism that generates non-zero p_T^Z , namely a recoil against hadronic emission from the partonic initial states. As a consequence, the ϕ_η^* distribution probes the same type of physics as the transverse momentum distribution. As we shall see in section 2, in the

small p_T^Z limit, ϕ_η^* is explicitly related to $p_T^Z/m_{\ell\ell}$ where $m_{\ell\ell}$ is the invariant mass of the lepton pair. Furthermore, ϕ_η^* is positive by construction and depends exclusively on the directions (rather than the magnitudes) of the lepton momenta. As the directions of the leptons are considerably better measured than their transverse momenta, analysing the low p_T^Z region with this angular kinematical variable ϕ_η^* has the potential to increase the accuracy of the measurements and opens up the possibility of making more stringent tests of the theoretical predictions for both observables.

So far, the ϕ_η^* distribution and related observables have been studied at the Tevatron by the D0 collaboration [14] and by the ATLAS Collaboration at the LHC at $\sqrt{s} = 7$ TeV [15] and $\sqrt{s} = 8$ TeV [2] and very recently by the LHCb Collaboration at 13 TeV [16]. The 7 TeV data from ATLAS have been compared with theoretical predictions from the Monte Carlo program RESBOS [17] which includes NLO fixed order corrections, resummation, and non-perturbative effects. The 7 TeV measurements have also been compared to the fixed order NNLO inclusive Z prediction of FEWZ [8] and to a matched NLO+NNLL resummed computation [18].

Even above $\phi_\eta^* \sim 0.1$, a relatively large value of ϕ_η^* , the NNLO predictions obtained with FEWZ undershoot the data by about ten percent. This is not a surprise given that although these predictions are NNLO accurate for the inclusive cross section, they are only NLO accurate for the ϕ_η^* distribution as for the p_T^Z -spectrum. The theoretical predictions for the NNLL resummed calculation matched to NLO fixed order show reasonable agreement with the data, but with large theoretical uncertainties. The ϕ_η^* measurements of ATLAS at 8 TeV [2] have thus so far only been compared with results obtained from parton shower Monte Carlo programs [19] and RESBOS.

It is the purpose of this paper to explore the production of lepton pairs at low (but non-zero) transverse momentum at NNLO for both the p_T^Z and ϕ_η^* distributions. In particular, we will make the first NNLO accurate predictions for observables related to ϕ_η^* at non-vanishing ϕ_η^* and make a direct comparison with the 8 TeV ATLAS p_T^Z and ϕ_η^* data [2] by using the same fiducial cuts for the leptons as those used in the experimental measurements. The NNLO predictions are obtained using our parton-level code NNLOJET, designed to compute NNLO corrections to observables related to Z + jet production [12], by being completely inclusive on the QCD radiation (i.e. dropping the requirement of observing a jet) and applying a low cut on either p_T^Z or ϕ_η^* . We make predictions for all but the first bin in p_T^Z (0–2 GeV) or ϕ_η^* (0–0.004) where the fixed order prediction for the distribution formally diverges.

As expected, in the very low transverse momentum domain, reliable theoretical predictions can only be provided through the resummation of large logarithms of the form $\ln^n(p_T^Z)$ or $\ln^n(\phi_\eta^*)$ to all orders in perturbation theory. We shall see these large logarithmic effects emerge from the fixed order distributions shown in section 3. Nevertheless, we find that the inclusion of the NNLO corrections to the normalised distributions accurately describe the data over a wide range of values of p_T^Z and ϕ_η^* . In particular, we will show that the NNLO fixed order predictions accurately describe the data to much lower values of p_T^Z and ϕ_η^* than the corresponding predictions obtained at NLO. By studying the form of the large logarithms we find an approximate relationship between the values of p_T^Z and

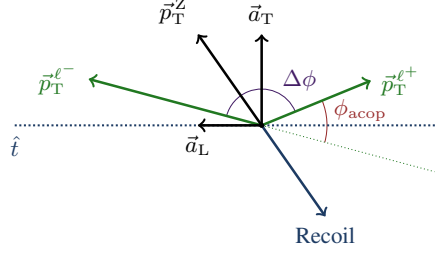


Figure 1. Illustration of the variables needed in the decomposition of the transverse momentum vector of the di-lepton system: \vec{p}_T^Z and the angles entering the definition of ϕ^* (see text). The hadronic recoil is expected to have an equal and opposite transverse momentum vector to that of the di-lepton system vector \vec{p}_T^Z .

ϕ_η^* where the fixed order distributions start to break down and find consistency between the two observables.

2 Kinematics of the angular variable ϕ_η^* in the low- p_T^Z regime

Let us first consider how the variable ϕ_η^* defined in Eq. (1.1) is related to the transverse momentum of the Z boson for events where the leptons are separated by an angle $\Delta\phi$ which is greater than $\pi/2$, cf. Refs. [13, 20]. This type of event is illustrated in Fig. 1. The transverse momentum vector of the di-lepton system, \vec{p}_T^Z , can be decomposed into orthogonal components with respect to an event axis in the plane transverse to the beam direction. The lepton thrust axis is defined by a unit vector \hat{t} ,

$$\hat{t} = \frac{(\vec{p}_T^{\ell-} - \vec{p}_T^{\ell+})}{|\vec{p}_T^{\ell-} - \vec{p}_T^{\ell+}|}, \quad (2.1)$$

where $\vec{p}_T^{\ell-}$ and $\vec{p}_T^{\ell+}$ are the lepton momentum vectors in the transverse plane. The longitudinal and transverse components of \vec{p}_T^Z are denoted by \vec{a}_L and \vec{a}_T . Their respective magnitudes denoted by a_L and a_T are related to p_T^Z by

$$p_T^Z = \sqrt{a_T^2 + a_L^2}. \quad (2.2)$$

We are particularly interested in the relation between the variables p_T^Z and ϕ_η^* when the Z boson transverse momentum is small. In the low p_T^Z limit we are in “quasi-Born-like” kinematics where the two leptons are almost back-to-back in the transverse plane and $\Delta\phi \approx \pi$. The magnitudes of the lepton momenta then satisfy

$$p_T^{\ell-} \approx p_T^{\ell+} \equiv p_T^\ell \gg p_T^Z \quad (2.3)$$

and the scattering angle behaves as

$$\sin(\theta_\eta^*) \approx \frac{2p_T^\ell}{m_{\ell\ell}}. \quad (2.4)$$

Furthermore, in this limit a_L and a_T are approximately given by

$$a_L^2 \equiv (p_T^Z)^2 \cos^2 \alpha \approx (p_T^{\ell^-} - p_T^{\ell^+})^2, \quad (2.5)$$

$$a_T^2 \equiv (p_T^Z)^2 \sin^2 \alpha \approx 2(p_T^\ell)^2(1 + \cos \Delta\phi), \quad (2.6)$$

where α is the angle between \vec{p}_T^Z and \hat{t} . Using the definition of ϕ_η^* in Eq. (1.2), in the small p_T^Z limit (i.e. $\Delta\phi \approx \pi$), we arrive at

$$\phi_\eta^* \approx \frac{a_T}{m_{\ell\ell}}, \quad (2.7)$$

where we have used

$$\tan\left(\frac{\phi_{\text{acop}}}{2}\right) \approx \frac{a_T}{2p_T^\ell}. \quad (2.8)$$

From Eq. (2.7), it is clear that in the small p_T^Z region, the ϕ_η^* distribution probes the same physics as the a_T and p_T^Z distributions (since $a_T = p_T^Z \sin \alpha$). In section 3.4 we will further establish a more direct relation between ϕ_η^* and p_T^Z by examining the arguments of the logarithms that appear in the respective resummation formulae.

3 Numerical results

The results presented in this section are based on the calculation of Ref. [12], where the NNLO QCD corrections to $Z + \text{jet}$ production were computed using the antenna subtraction formalism [21] to isolate the infrared singularities in the different Z -boson-plus-jet contributions. Our calculation is implemented in a newly developed parton-level Monte Carlo generator NNLOJET. This program provides the necessary infrastructure for the antenna subtraction of hadron collider processes at NNLO and performs the integration of all contributing subprocesses at this order. Components of it have also been used in other NNLO QCD calculations [11, 12, 22–26] using the antenna subtraction method. Other processes can be added to NNLOJET provided the matrix elements are available.

In Refs. [11, 27], we showed that NNLOJET can be used to predict the Z -boson p_T spectrum to genuine NNLO accuracy by dropping the requirement of observing a jet and instead imposing a finite cut on the transverse momentum $p_T^Z > p_{T,\text{cut}}^Z$. These predictions are therefore completely inclusive on the QCD radiation and depend only on the fiducial cuts applied to the leptons. This calculation is extended in this work to substantially lower values of p_T^Z . Since the ϕ_η^* variable is related to p_T^Z , we can equally use NNLOJET to compute the the first NNLO accurate predictions for $\phi_\eta^* > \phi_{\eta,\text{cut}}^*$ in the same way. By going to low values of p_T^Z or ϕ_η^* , one starts to resolve the N^3LO infrared singularity at $p_T^Z = 0$ or $\phi_\eta^* = 0$ which presents a challenge for any NNLO subtraction or slicing method.

3.1 Calculational setup

The ATLAS collaboration measured [2] the p_T^Z and ϕ_η^* distributions at 8 TeV by applying fiducial acceptance cuts on the leptons:

$$|\eta^{\ell^\pm}| < 2.4, \quad p_T^{\ell^\pm} > 20 \text{ GeV}, \quad 46 \text{ GeV} < m_{\ell\ell} < 150 \text{ GeV}, \quad |y^Z| < 2.4, \quad (3.1)$$

where y^Z denotes the rapidity of the lepton pair. We apply the same cuts in our calculation. As discussed above, a non-zero cut $\phi_\eta^* > \phi_{\eta,\text{cut}}^*$ or $p_T^Z > p_{T,\text{cut}}^Z$ has to be applied in order to render the $Z + \text{jet}$ calculation infrared safe. We choose the value $\phi_{\eta,\text{cut}}^* = 0.004$ for the ϕ_η^* distribution and $p_{T,\text{cut}}^Z = 2$ GeV for the p_T^Z distribution, each time corresponding to the upper edge of the first bin in the ATLAS data set.

For our numerical computations, we use the NNPDF3.0 parton distribution functions [28] with the value of $\alpha_s(M_Z) = 0.118$ at NNLO, and $M_Z = 91.1876$ GeV. Note that we systematically use the same set of PDFs and the same value of $\alpha_s(M_Z)$ for the NLO and NNLO predictions. The factorisation and renormalisation scales are chosen dynamically on an event-by-event basis using the central scale

$$\mu_0 \equiv \sqrt{m_{\ell\ell}^2 + (p_T^Z)^2}, \quad (3.2)$$

where $m_{\ell\ell}$ is the invariant mass of the final state lepton pair. The theoretical uncertainty is estimated using the standard 7-point scale variation, i.e. varying μ_R and μ_F independently about μ_0 by multiplicative factors in the range $[1/2, 2]$ while retaining $1/2 < \mu_R/\mu_F < 2$. We restrict our discussion to normalised distributions which are much more precisely determined due to the fact that systematic errors such as the luminosity uncertainties cancel in the ratio. To this end, we use the implementation of the NNLO QCD corrections to inclusive Z/γ^* production available in NNLOJET to compute the fiducial cross section for the respective bins.

The measurement of the p_T^Z and ϕ_η^* distributions in Ref. [2] are performed multi-differentially with additional binning in the invariant mass ($m_{\ell\ell}$) and the rapidity (y^Z) of the lepton pair. The invariant-mass range of Eq. (3.1) is divided into three mass bins: the Z resonance bin containing the Z -boson peak ($m_{\ell\ell} \in [66, 116]$ GeV) and two off-resonance bins covering the low-mass ($m_{\ell\ell} \in [46, 66]$ GeV) and high-mass ($m_{\ell\ell} \in [116, 150]$ GeV) regions. Each mass bin is further subdivided into equal-sized rapidity bins—six for the resonance region and three for each of the off-resonance regions. The ATLAS measurement of the p_T^Z distribution [2] further extends to lower invariant masses, with three more bins in the range below 46 GeV. For those bins, results are provided only for $p_T^Z > 45$ GeV, which have been studied to NNLO accuracy already in Ref. [11].

3.2 The transverse momentum distribution at low p_T^Z

The ATLAS measurement of the transverse momentum distribution [2] starts at vanishing transverse momentum, with the first bin covering the range $p_T^Z \in [0, 2]$ GeV. In this bin, the NNLO calculation of Z production at finite transverse momentum diverges, and would need to be combined with the $N^3\text{LO}$ three-loop contribution to inclusive Z production, which is beyond the scope and aims of this study.

The measured p_T^Z distribution is compared to the NLO and NNLO predictions in Figs. 2, 3. Note that the theory uncertainties shown in these figures are estimated using a 3-point scale variation instead of the 7-point variation described above by restricting to the case $\mu_F \equiv \mu_R$. As already observed in Ref. [11], the NLO calculation does not describe the shape of the data below $p_T^Z \approx 40$ GeV, while the NNLO calculation agrees with the data

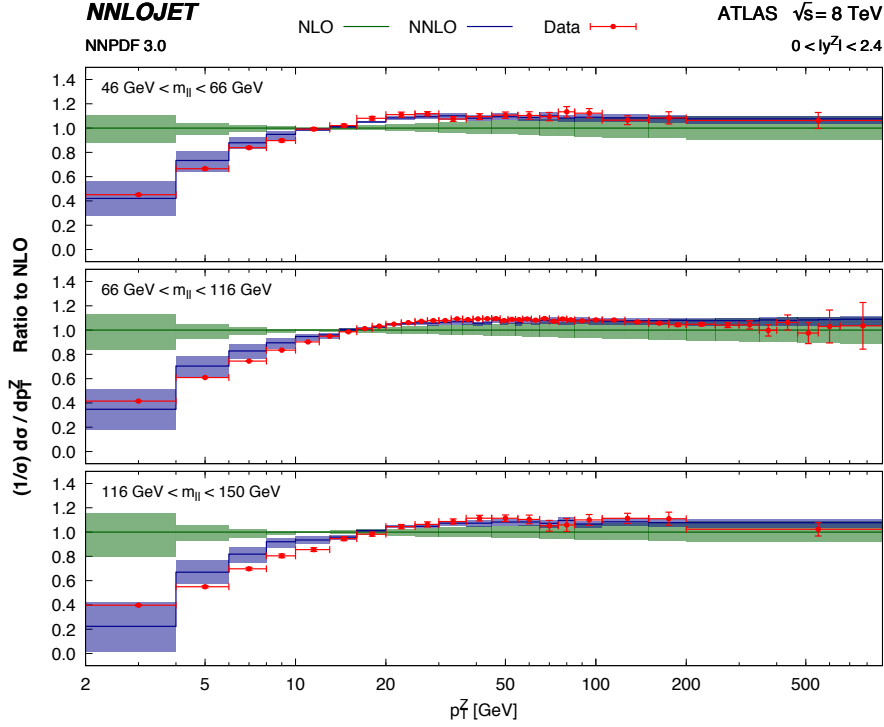


Figure 2. Normalized transverse momentum distribution differential in $m_{\ell\ell}$ at NLO and NNLO compared to ATLAS data [2]. The distribution is normalised to the NLO prediction. The green bands denote the NLO prediction with scale uncertainty and the blue bands show the NNLO prediction with scale uncertainty.

down to substantially lower values of p_T^Z . With the extended range in p_T^Z that is covered in this study, we can now quantify this agreement in observing that the shape of the data is well-reproduced by the NNLO calculation down to $p_T^Z \approx 4$ GeV. A deviation for lower values of p_T^Z is expected due to the onset of large logarithmic corrections proportional to powers of $\ln(p_T^Z/m_{\ell\ell})$ in all orders in the strong coupling, which necessitates logarithmic resummation. The three data bins below this value are however insufficient to resolve and quantify this potential deviation in detail. In this region, the determination of p_T^Z is limited by the experimental lepton energy resolution. A more detailed picture can be gained from the distribution in the ϕ_η^* variable, which is determined using the lepton angles rather than their energies. This distribution is discussed in detail in the next two subsections.

3.3 The large ϕ_η^* region

We first consider the region of large ϕ_η^* values: $\phi_\eta^* > 0.051$, where one expects that the perturbative prediction is not dominated by large logarithms. Figure 4 shows the ratio of the normalised fixed-order predictions to the NLO prediction for the ϕ_η^* distribution for each of the six rapidity slices in the on-resonance $m_{\ell\ell}$ -bin. For $\phi_\eta^* \gtrsim 0.2$, the NLO predictions systematically undershoot the data points by almost 5–10%. This is reminiscent of the behaviour of the NLO prediction for the p_T^Z distribution. The NNLO corrections are

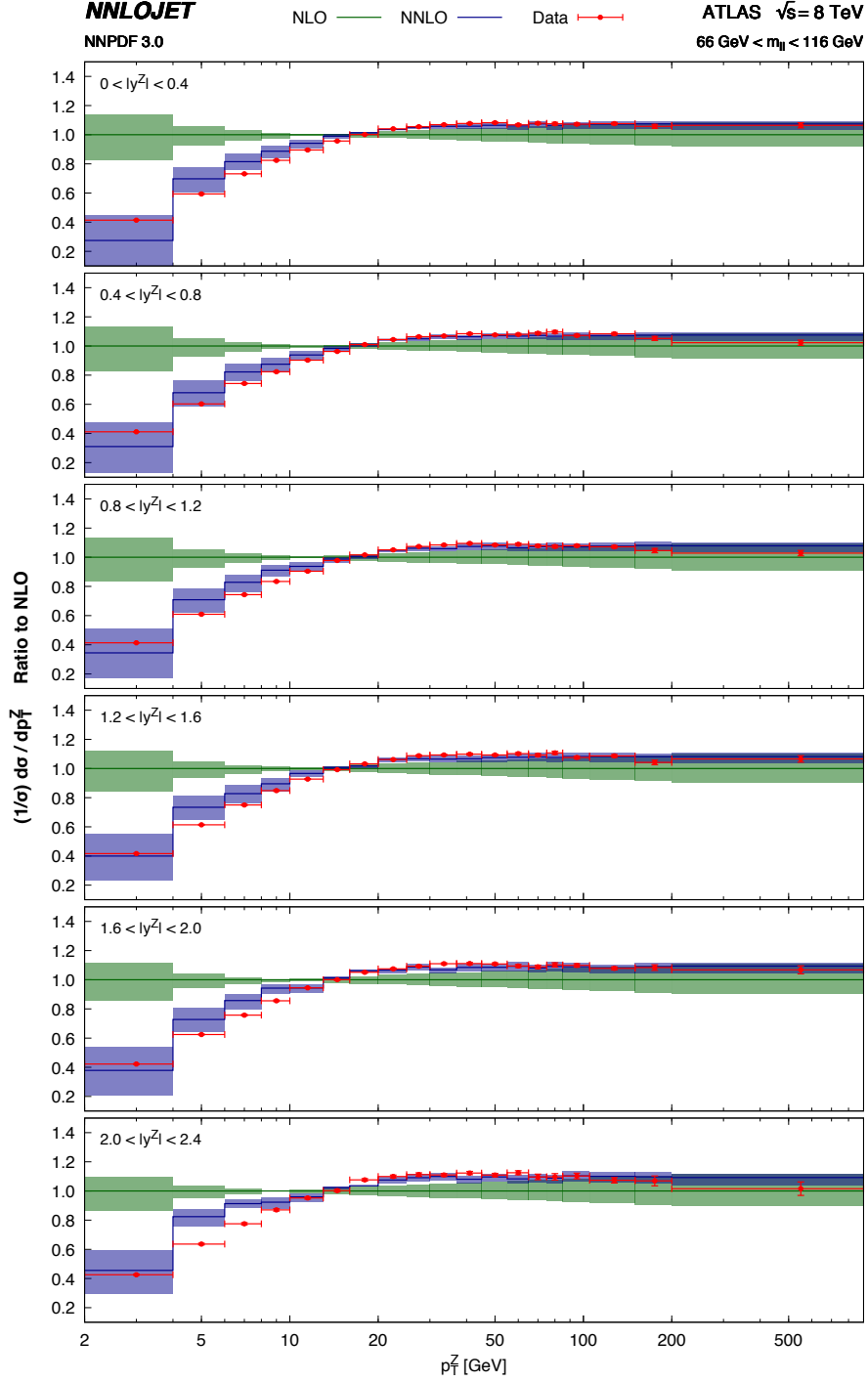


Figure 3. Normalized transverse momentum distribution differential in y^Z for the on-resonance bin at NLO and NNLO compared to ATLAS data [2]. The distribution is normalised to the NLO prediction. The green bands denote the NLO prediction with scale uncertainty and the blue bands show the NNLO prediction with scale uncertainty.

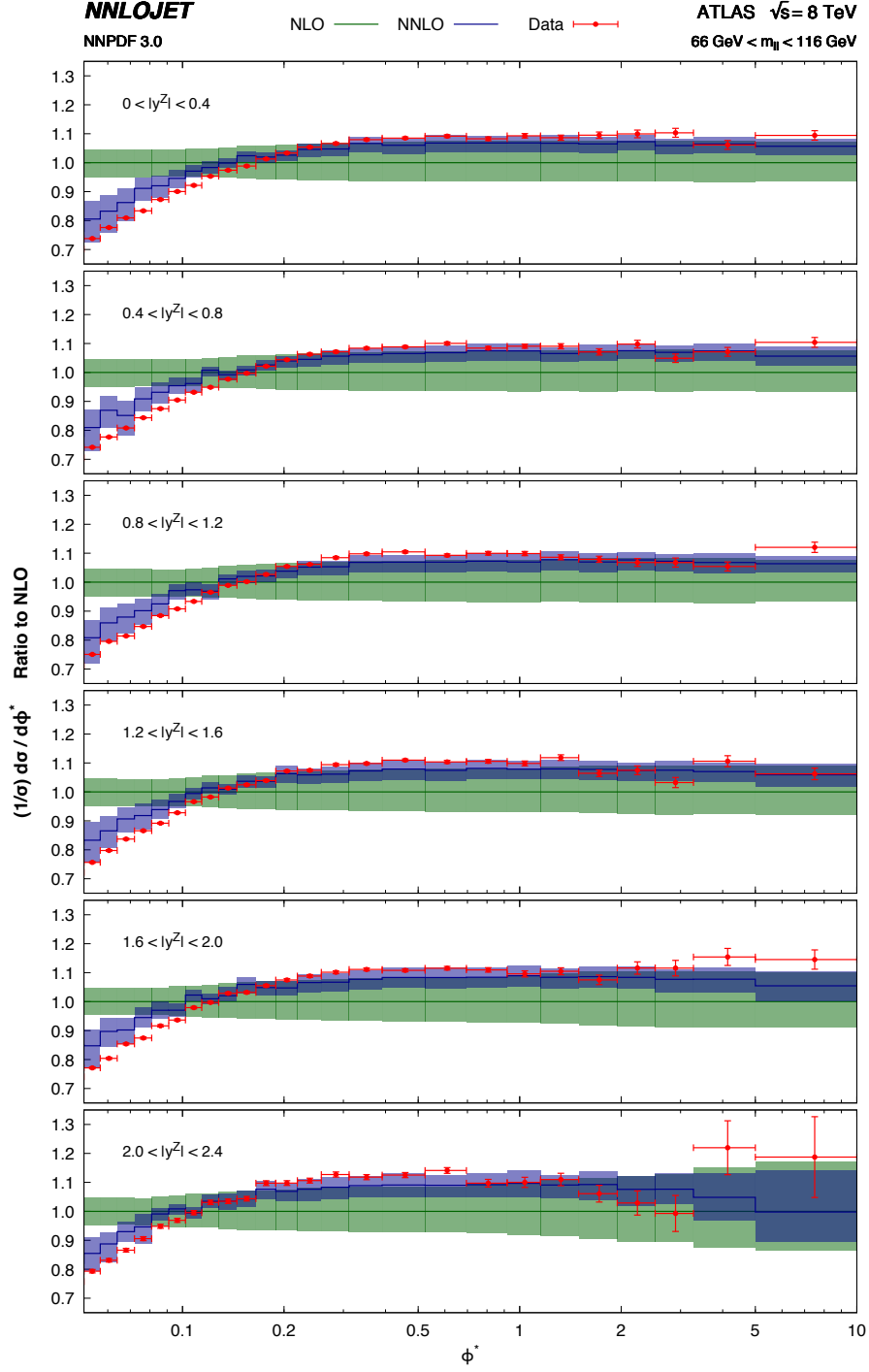


Figure 4. The ϕ_η^* distribution for $\phi_\eta^* > 0.051$ for the on-resonance region $66 \text{ GeV} < m_{\ell\ell} < 116 \text{ GeV}$ in 6 different rapidity slices. The distribution is normalised to the NLO prediction. The green bands denote the NLO prediction with scale uncertainty and the blue bands show the NNLO prediction with scale uncertainty.

positive in this region and lead to a significant improvement in the theory–data comparison. Moreover, the residual scale uncertainty is greatly reduced by moving from NLO to NNLO. Below $\phi_\eta^* \approx 0.1$ the shape of the NLO prediction quickly deviates away from the data points by more than 30–40% for $\phi_\eta^* \lesssim 0.051$. This divergent behaviour is tamed by the inclusion of the NNLO corrections where the shape of the data points is well captured by the theory curve down to small values of $\phi_\eta^* \approx 0.051$.

Figure 5 shows the ϕ_η^* distribution for the two off-resonance $m_{\ell\ell}$ bins where the top and bottom plots in the figure correspond to the low-mass and high-mass bins, respectively. Due to lower event rates away from the Z-boson resonance region, the statistical errors on the experimental data points are significantly larger than the on-resonance results of Fig. 4. The qualitative picture, however, is very similar with a better theory–data agreement in the high- ϕ_η^* region and a very much improved prediction of the shape down to low values of $\phi_\eta^* \approx 0.051$.

3.4 The small ϕ_η^* region

At smaller values of ϕ_η^* , we enter the domain of the large logarithms where the fixed-order perturbative prediction breaks down. In this kinematical limit, ϕ_η^* and p_T^Z are closely related, as can be seen both from the structure of the logarithmically enhanced terms in the respective cross sections and from simple kinematical considerations.

The leading logarithmic behaviour of the transverse momentum distribution is obtained by resumming terms of the form $\alpha_s^n \ln^{(2n)}(p_T^Z/m_{\ell\ell})$ to all orders. By expanding the resummed expression up to $\mathcal{O}(\alpha_s^2)$, one obtains [29] the coefficients of the leading logarithms in the fixed order NLO and NNLO predictions for the normalised p_T^Z distribution:

$$p_T^Z \left(\frac{1}{\sigma_0} \frac{d\sigma}{dp_T^Z} \right)_{\text{LL, expanded}} = -4C_F \frac{\alpha_s}{\pi} \ln \left(\frac{(p_T^Z)^2}{m_{\ell\ell}^2} \right) + 2C_F^2 \left(\frac{\alpha_s}{\pi} \right)^2 \ln^3 \left(\frac{(p_T^Z)^2}{m_{\ell\ell}^2} \right) + \mathcal{O}(\alpha_s^3). \quad (3.3)$$

The resummation of the a_T distribution (see Eq. (2.5)) has been studied in Refs. [30, 31]. Expanding the resummed expression, we find

$$a_T \left(\frac{1}{\sigma_0} \frac{d\sigma}{da_T} \right)_{\text{LL, expanded}} = -4C_F \frac{\alpha_s}{\pi} \ln \left(\frac{4a_T^2}{m_{\ell\ell}^2} \right) + 2C_F^2 \left(\frac{\alpha_s}{\pi} \right)^2 \ln^3 \left(\frac{4a_T^2}{m_{\ell\ell}^2} \right) + \mathcal{O}(\alpha_s^3). \quad (3.4)$$

Using the relation between ϕ_η^* and a_T (2.7) as $\phi_\eta^* \sim a_T/m_{\ell\ell}$ gives the leading-logarithmic behaviour of the ϕ_η^* distribution as

$$\phi_\eta^* \left(\frac{1}{\sigma_0} \frac{d\sigma}{d\phi_\eta^*} \right)_{\text{LL, expanded}} = -4C_F \frac{\alpha_s}{\pi} \ln (4(\phi_\eta^*)^2) + 2C_F^2 \left(\frac{\alpha_s}{\pi} \right)^2 \ln^3 (4(\phi_\eta^*)^2) + \mathcal{O}(\alpha_s^3). \quad (3.5)$$

Comparing the arguments of the logarithms in Eqs. (3.3) and (3.5), we can establish a relation between the dominant logarithmic behaviour of the p_T^Z and ϕ_η^* distributions through the correspondence

$$2\phi_\eta^* \approx p_T^Z/m_{\ell\ell}, \quad (3.6)$$

which holds in the region of small ϕ_η^* and small p_T^Z . The same relation can be established kinematically by considering the di-lepton pair of invariant mass $m_{\ell\ell}$ produced at central

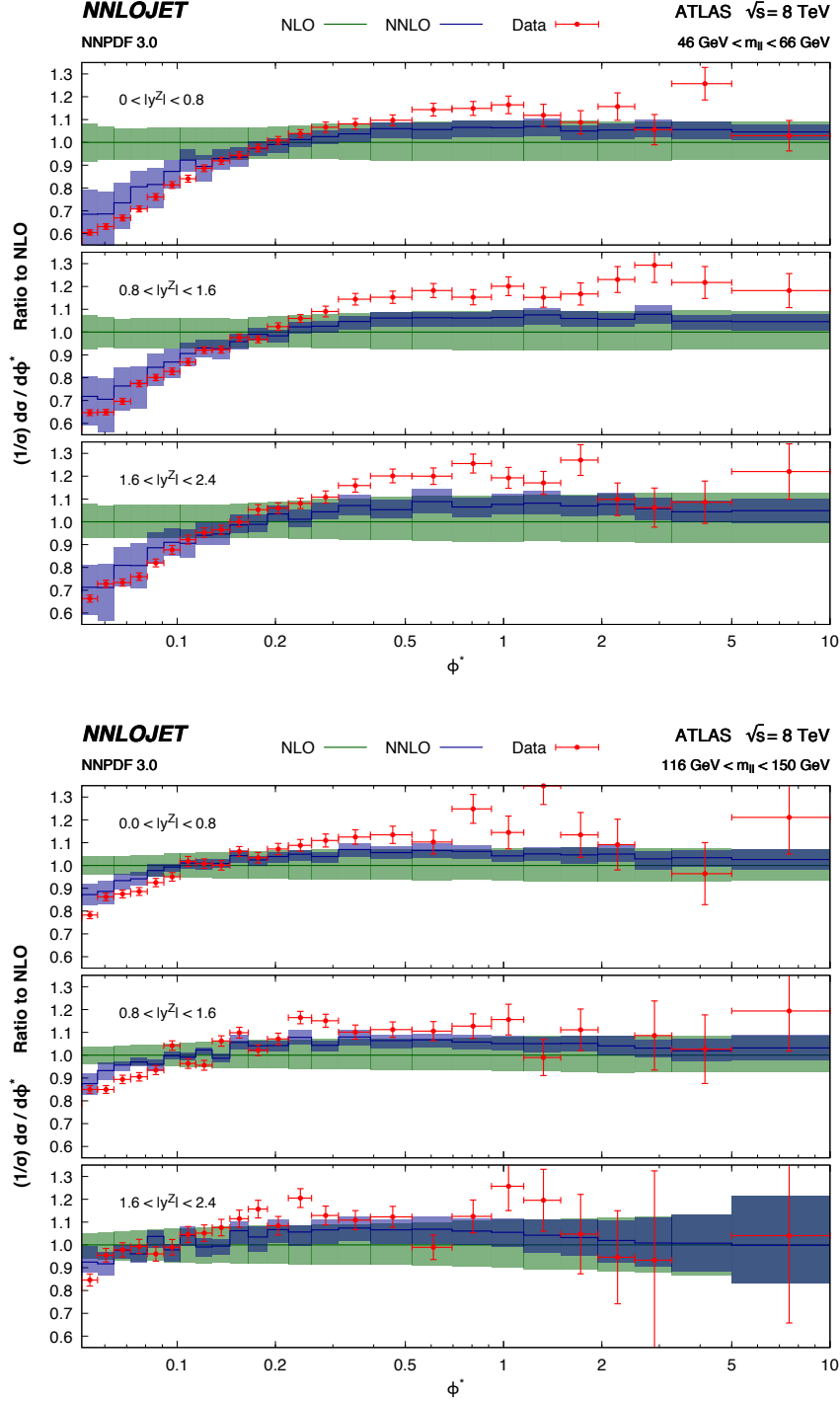


Figure 5. The ϕ_η^* distribution for $\phi_\eta^* > 0.051$ for the two off-resonance $m_{\ell\ell}$ bins, $46 \text{ GeV} < m_{\ell\ell} < 66 \text{ GeV}$ (top) and $116 \text{ GeV} < m_{\ell\ell} < 150 \text{ GeV}$ (bottom) in 3 different rapidity slices. The distribution is normalised to the NLO prediction. The green bands denote the NLO prediction with scale uncertainty and the blue bands show the NNLO prediction with scale uncertainty.

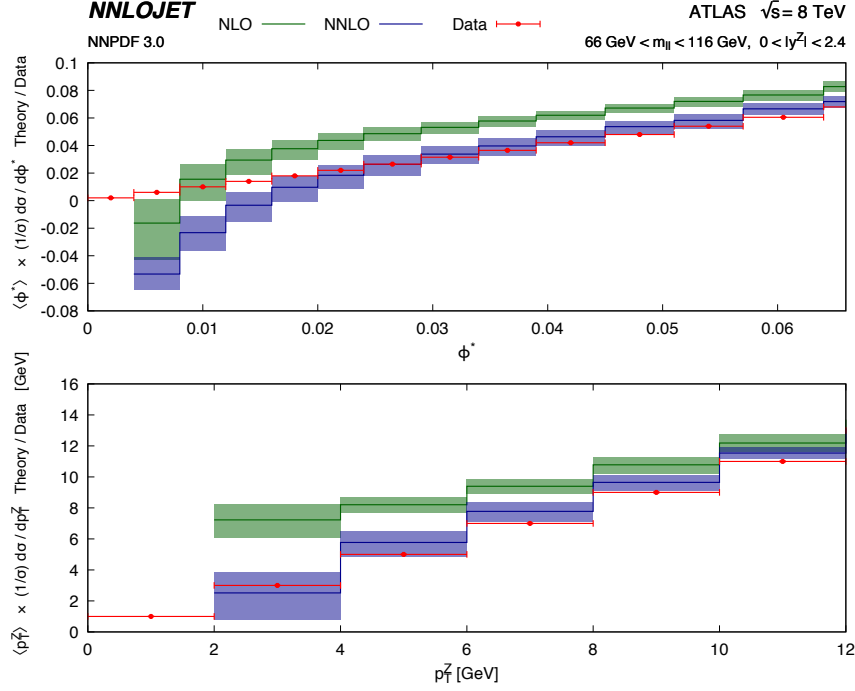


Figure 6. The ϕ_η^* distribution for $\phi_\eta^* > \phi_{\eta,\text{cut}}^*$ for the on-resonance mass bin $66 \text{ GeV} < m_{\ell\ell} < 116 \text{ GeV}$. The distribution is normalised to the experimental data. The green bands denote the NLO prediction with scale uncertainty and the blue bands show the NNLO prediction with scale uncertainty.

rapidity and with transverse momentum p_T^Z and expanding in the momentum difference in the lepton momenta. Note that relation (3.6) is based on comparing the leading logarithmic behaviour of the p_T^Z and ϕ_η^* distributions. Beyond the leading logarithmic approximation, these distributions differ substantially as studied in Refs. [30, 31].

The above considerations suggest that the distributions in ϕ_η^* and p_T^Z are closely related in the infrared region. In particular, one should expect the onset of large logarithmic corrections (and consequently the breakdown of the fixed order NLO and NNLO predictions) to occur roughly simultaneously at values of ϕ_η^* and p_T^Z related through Eq. (3.6). To test this hypothesis, we superimpose the infrared regions of these distributions (for the three mass bins) in Figs. 6–8. For better visibility over the kinematical range, we show

$$\langle \mathcal{O} \rangle_{\text{bin}} \times \frac{\frac{1}{\sigma} \frac{d\sigma}{d\mathcal{O}}|_{\text{Theory}}}{\frac{1}{\sigma} \frac{d\sigma}{d\mathcal{O}}|_{\text{Data}}} \quad \text{with} \quad \mathcal{O} = \phi_\eta^*, p_T^Z,$$

i.e. the ratio of normalised distributions weighted by the central bin values. The p_T^Z range is fixed to $[0, 12] \text{ GeV}$, while the ϕ_η^* range is chosen according to Eq. (3.6) for each mass bin, using the central value of $m_{\ell\ell}$. The first bins contain the zero value and are not accessible by a fixed-order calculation of the p_T^Z or ϕ_η^* distributions, which diverges there.

First and foremost, we observe the substantially higher experimental resolution in ϕ_η^* : in the region covered by $(5 + 1)$ bins in p_T^Z , the ϕ_η^* distribution contains $(12 + 1)$ bins

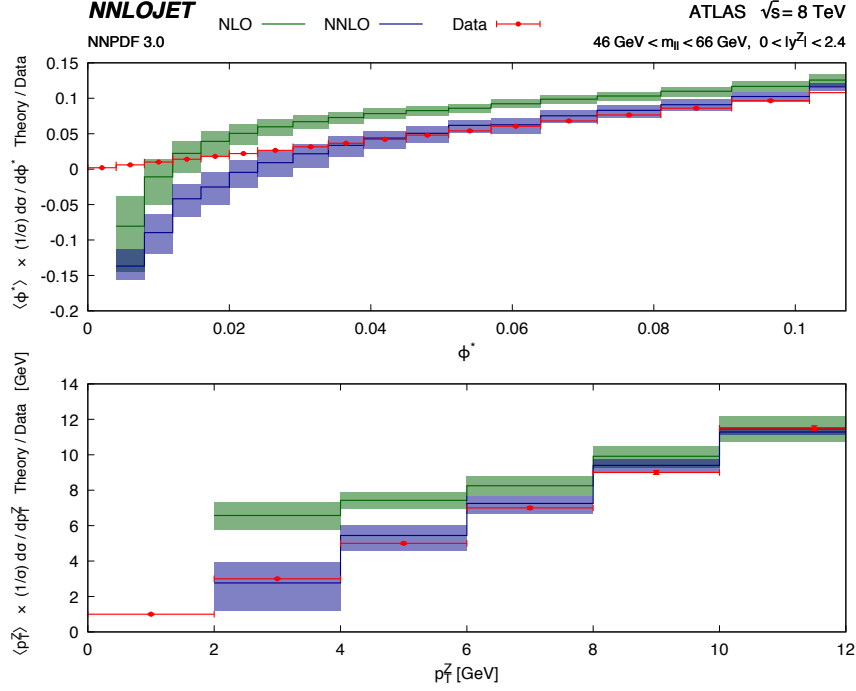


Figure 7. The ϕ_η^* distribution for $\phi_\eta^* > \phi_{\eta,\text{cut}}^*$ for the below resonance mass bin $46 \text{ GeV} < m_{\ell\ell} < 66 \text{ GeV}$. The distribution is normalised to the experimental data. The green bands denote the NLO prediction with scale uncertainty and the blue bands show the NNLO prediction with scale uncertainty.

on-resonance, $(16+1)$ bins below-resonance and $(9+1)$ bins above-resonance. This reflects the much better experimental resolution of the low p_T^Z region afforded by the ϕ_η^* variable.

We see that the NLO prediction does not describe the data in the plotting range for all three mass bins and in fact only starts to describe the data at larger values of p_T^Z and ϕ_η^* which are tabulated in Table 1. However, we observe that the NNLO description remains reliable down to values of $\phi_\eta^* \approx 0.02$ (also shown in Table 1). The precise point of deviation in the p_T^Z distributions cannot be resolved due to the coarse binning. Nevertheless, these values of ϕ_η^* and p_T^Z where the fixed order predictions start to deviate from the data appear to be in line with the expectation from Eq. (3.6). In other words, the places where the large logarithms in the fixed order perturbative predictions start to emerge (and therefore need resummation) in each distribution are consistent with the relationship $p_T^Z \sim 2m_{\ell\ell}\phi_\eta^*$.

4 Summary and conclusions

We have studied the NNLO QCD corrections to the Drell–Yan production of lepton pairs at small transverse momentum, inclusive over the hadronic final state. There are two relevant observables, p_T^Z and ϕ_η^* . From the experimental point of view, ϕ_η^* relies on knowing the lepton direction and can be measured more precisely at low transverse momentum than p_T^Z where the momenta of the final state leptons largely cancel.

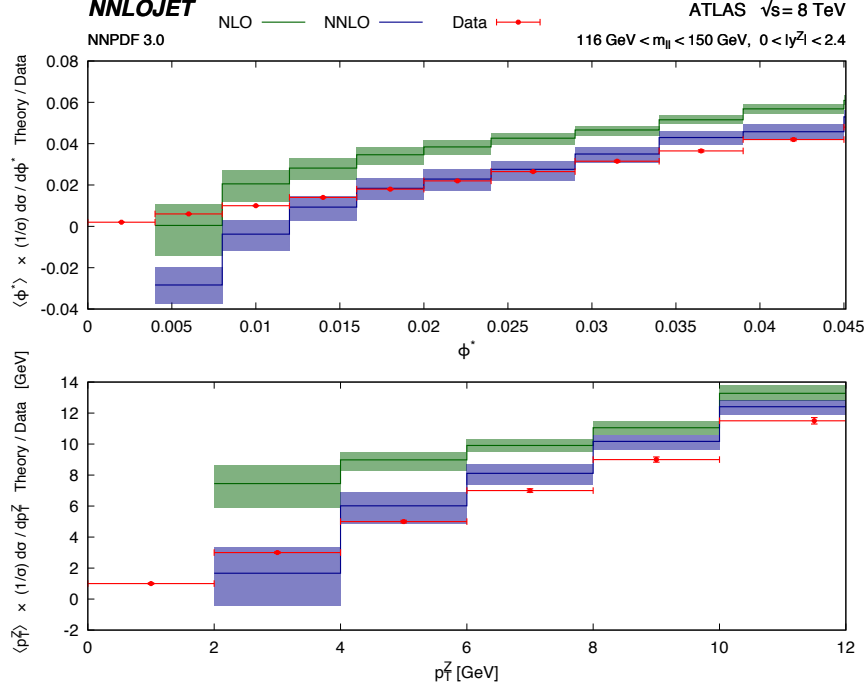


Figure 8. The ϕ_η^* distribution for $\phi_\eta^* > \phi_{\eta, \text{cut}}^*$ for the above resonance mass bin $116 \text{ GeV} < m_{\ell\ell} < 150 \text{ GeV}$. The distribution is normalised to the experimental data. The green bands denote the NLO prediction with scale uncertainty and the blue bands show the NNLO prediction with scale uncertainty.

	$m_{\ell\ell}\text{-bin [GeV]}$	$\phi_{\eta, \text{depart}}^*$	$p_{T, \text{depart}}^Z$	$2 \langle m_{\ell\ell} \rangle \phi_{\eta, \text{depart}}^*$
NLO	46–66	~ 0.14	$\sim 10 \text{ GeV}$	16 GeV
	66–116	~ 0.11	$\sim 14 \text{ GeV}$	20 GeV
	116–150	~ 0.08	$\sim 16 \text{ GeV}$	21 GeV
NNLO	46–66	~ 0.028	$\lesssim 3 \text{ GeV}$	3.1 GeV
	66–116	~ 0.018	$\lesssim 3 \text{ GeV}$	3.3 GeV
	116–150	~ 0.014	$\sim 4 \text{ GeV}$	3.9 GeV

Table 1. Values of $\phi_{\eta, \text{depart}}^*$ and $p_{T, \text{depart}}^Z$ for the three mass windows corresponding to the values of ϕ_η^* and p_T^Z where the fixed order predictions of the distributions start to deviate from the experimental data.

Our calculation is performed using the parton-level Monte Carlo generator NNLOJET which implements the antenna subtraction method for NNLO calculations of hadron collider observables. It extends our earlier calculations of $Z/\gamma^* + \text{jet}$ production [12] and Z/γ^* production at large transverse momentum [11]. We have performed a thorough comparison of theory predictions to the 8 TeV Run 1 data of the LHC for cross sections defined over a fiducial region of lepton kinematics from the ATLAS [2] collaboration.

At large values of ϕ_η^* , we observe that the NNLO corrections to the distribution normalised to the inclusive NNLO dilepton cross section are moderate and positive, resulting in an excellent agreement between data and theory. This agreement holds across the three $m_{\ell\ell}$ bins and for all slices in y^Z .

In the small transverse momentum region, we expect the fixed order calculation to break down due to the emergence of large logarithmic corrections of the form $\alpha_s^n \log^{2n-1}(p_T^Z)$ or $\alpha_s^n \log^{2n-1}(\phi_\eta^*)$. Nevertheless, the inclusion of the NNLO contributions increases the domain of validity of the fixed order calculation and we showed that the fixed order perturbative predictions start to break down at $p_T^Z \sim 4$ GeV (20 GeV), $\phi_\eta^* \sim 0.02$ (0.1) at NNLO (NLO). We also showed that these breakdown points satisfy an approximate relationship $p_T^Z \sim 2m_{\ell\ell}\phi_\eta^*$ that is motivated by considering the form of the leading logarithms.

The NNLO corrections improve the perturbative description of the p_T^Z and ϕ_η^* distributions by (a) reducing the theoretical scale uncertainty and (b) increasing the kinematic range in p_T^Z and ϕ_η^* that the fixed order prediction can describe. We anticipate that this calculation will allow a consistent inclusion of the precision data on the Z transverse momentum distribution into NNLO determinations of parton distributions and the strong coupling constant.

Acknowledgments

The authors thank Xuan Chen, Juan Cruz-Martinez, James Currie, Jan Niehues and Joao Pires for useful discussions and their many contributions to the NNLOJET code. We gratefully acknowledge the computing resources provided by the WLCG through the GridPP Collaboration. This research was supported in part by the National Science Foundation under Grant NSF PHY11-25915, in part by the Swiss National Science Foundation (SNF) under contracts 200020-162487 and CRSII2-160814, in part by the UK Science and Technology Facilities Council, in part by the Research Executive Agency (REA) of the European Union under the Grant Agreement PITN-GA-2012-316704 (“HiggsTools”) and the ERC Advanced Grant MC@NNLO (340983).

References

- [1] G. Aad *et al.* [ATLAS Collaboration], JHEP **1409** (2014) 145 [arXiv:1406.3660 [hep-ex]].
- [2] G. Aad *et al.* [ATLAS Collaboration], Eur. Phys. J. C **76** (2016) 291 [arXiv:1512.02192 [hep-ex]].
- [3] S. Chatrchyan *et al.* [CMS Collaboration], Phys. Rev. D **85** (2012) 032002 [arXiv:1110.4973 [hep-ex]].

- [4] V. Khachatryan *et al.* [CMS Collaboration], Phys. Lett. B **749** (2015) 187 [arXiv:1504.03511 [hep-ex]].
- [5] R. Aaij *et al.* [LHCb Collaboration], JHEP **1508** (2015) 039 [arXiv:1505.07024 [hep-ex]]; JHEP **1601** (2016) 155 [arXiv:1511.08039 [hep-ex]].
- [6] R. Hamberg, W. L. van Neerven and T. Matsuura, Nucl. Phys. B **359** (1991) 343 [Nucl. Phys. B **644** (2002) 403]. W. L. van Neerven and E. B. Zijlstra, A Nucl. Phys. B **382** (1992) 11 [Nucl. Phys. B **680** (2004) 513]. C. Anastasiou, L. J. Dixon, K. Melnikov and F. Petriello, Phys. Rev. Lett. **91** (2003) 182002 [hep-ph/0306192]; K. Melnikov and F. Petriello, Phys. Rev. Lett. **96** (2006) 231803 [hep-ph/0603182]; Phys. Rev. D **74** (2006) 114017 [hep-ph/0609070]; S. Catani, G. Ferrera and M. Grazzini, JHEP **1005** (2010) 006 [arXiv:1002.3115 [hep-ph]].
- [7] S. Catani, L. Cieri, G. Ferrera, D. de Florian and M. Grazzini, Phys. Rev. Lett. **103** (2009) 082001 [arXiv:0903.2120 [hep-ph]].
- [8] R. Gavin, Y. Li, F. Petriello and S. Quackenbush, Comput. Phys. Commun. **182** (2011) 2388 [arXiv:1011.3540 [hep-ph]].
- [9] C. Anastasiou, L. J. Dixon, K. Melnikov and F. Petriello, Phys. Rev. D **69** (2004) 094008 [hep-ph/0312266].
- [10] J. C. Collins, D. E. Soper and G. F. Sterman, Nucl. Phys. B **250** (1985) 199; G. Bozzi, S. Catani, G. Ferrera, D. de Florian and M. Grazzini, Nucl. Phys. B **815** (2009) 174 [arXiv:0812.2862 [hep-ph]]; Phys. Lett. B **696** (2011) 207 [arXiv:1007.2351 [hep-ph]]; T. Becher and M. Neubert, Eur. Phys. J. C **71** (2011) 1665 [arXiv:1007.4005 [hep-ph]].
- [11] A. Gehrmann-De Ridder, T. Gehrmann, E. W. N. Glover, A. Huss and T. A. Morgan, JHEP **1607** (2016) 133 [arXiv:1605.04295 [hep-ph]].
- [12] A. Gehrmann-De Ridder, T. Gehrmann, E. W. N. Glover, A. Huss and T. A. Morgan, Phys. Rev. Lett. **117** (2016) 022001 [arXiv:1507.02850 [hep-ph]]; arXiv:1601.04569 [hep-ph].
- [13] A. Banfi, S. Redford, M. Vesterinen, P. Waller and T. R. Wyatt, Eur. Phys. J. C **71**, 1600 (2011) [arXiv:1009.1580 [hep-ex]].
- [14] V. M. Abazov *et al.* [D0 Collaboration], Phys. Rev. Lett. **106** (2011) 122001 [arXiv:1010.0262 [hep-ex]].
- [15] G. Aad *et al.* [ATLAS Collaboration], Phys. Lett. B **720** (2013) 32 [arXiv:1211.6899 [hep-ex]].
- [16] R. Aaij *et al.* [LHCb Collaboration], arXiv:1607.06495 [hep-ex].
- [17] C. Balazs and C. P. Yuan, Phys. Rev. D **56** (1997) 5558 [hep-ph/9704258], M. Guzzi, P. M. Nadolsky and B. Wang, Phys. Rev. D **90** (2014) 014030 [arXiv:1309.1393 [hep-ph]].
- [18] A. Banfi, M. Dasgupta, S. Marzani and L. Tomlinson, Phys. Lett. B **715** (2012) 152 [arXiv:1205.4760 [hep-ph]].
- [19] S. Alioli, P. Nason, C. Oleari and E. Re, JHEP **1006** (2010) 043 [arXiv:1002.2581 [hep-ph]], T. Sjostrand, S. Mrenna and P. Z. Skands, Comput. Phys. Commun. **178** (2008) 852 [arXiv:0710.3820 [hep-ph]], T. Gleisberg, S. Hoeche, F. Krauss, M. Schonherr, S. Schumann, F. Siegert and J. Winter, JHEP **0902** (2009) 007 [arXiv:0811.4622 [hep-ph]], S. Frixione and B. R. Webber, JHEP **0206** (2002) 029 [hep-ph/0204244].
- [20] M. Vesterinen and T. R. Wyatt, Nucl. Instrum. Meth. A **602** (2009) 432 [arXiv:0807.4956 [hep-ex]].

- [21] A. Gehrmann-De Ridder, T. Gehrmann and E. W. N. Glover, JHEP **0509** (2005) 056 [hep-ph/0505111]; Phys. Lett. B **612** (2005) 49 [hep-ph/0502110]; Phys. Lett. B **612** (2005) 36 [hep-ph/0501291]. A. Daleo, T. Gehrmann and D. Maitre, JHEP **0704** (2007) 016 [hep-ph/0612257]; A. Daleo, A. Gehrmann-De Ridder, T. Gehrmann and G. Luisoni, JHEP **1001** (2010) 118 [arXiv:0912.0374 [hep-ph]]; T. Gehrmann and P.F. Monni, JHEP **1112** (2011) 049 [arXiv:1107.4037 [hep-ph]]; R. Boughezal, A. Gehrmann-De Ridder and M. Ritzmann, JHEP **1102** (2011) 098 [arXiv:1011.6631 [hep-ph]]; A. Gehrmann-De Ridder, T. Gehrmann and M. Ritzmann, JHEP **1210** (2012) 047 [arXiv:1207.5779 [hep-ph]]; J. Currie, E.W.N. Glover and S. Wells, JHEP **1304** (2013) 066 [arXiv:1301.4693 [hep-ph]].
- [22] A. Gehrmann-De Ridder, T. Gehrmann, E.W.N. Glover and G. Heinrich, JHEP **0711** (2007) 058 [arXiv:0710.0346 [hep-ph]]; Comput. Phys. Commun. **185** (2014) 3331 [arXiv:1402.4140 [hep-ph]].
- [23] A. Gehrmann-De Ridder, T. Gehrmann, E.W.N. Glover and J. Pires, Phys. Rev. Lett. **110** (2013) 162003 [arXiv:1301.7310 [hep-ph]]; J. Currie, A. Gehrmann-De Ridder, E.W.N. Glover and J. Pires, JHEP **1401** (2014) 110 [arXiv:1310.3993 [hep-ph]].
- [24] X. Chen, T. Gehrmann, E.W.N. Glover and M. Jaquier, Phys. Lett. B **740** (2015) 147 [arXiv:1408.5325 [hep-ph]]; X. Chen, J. Cruz-Martinez, T. Gehrmann, E. W. N. Glover and M. Jaquier, [arXiv:1607.08817 [hep-ph]].
- [25] G. Abelof, A. Gehrmann-De Ridder and I. Majer, JHEP **1512** (2015) 074 [arXiv:1506.04037 [hep-ph]].
- [26] J. Currie, T. Gehrmann and J. Niehues, Phys. Rev. Lett. **117** (2016) 042001 [arXiv:1606.03991 [hep-ph]].
- [27] A. Gehrmann-De Ridder, T. Gehrmann, E. W. N. Glover, A. Huss and T. A. Morgan, arXiv:1607.01749 [hep-ph], to appear in Proceedings of Moriond 2016.
- [28] R. D. Ball *et al.* [NNPDF Collaboration], JHEP **1504** (2015) 040 [arXiv:1410.8849 [hep-ph]].
- [29] S. Catani, L. Cieri, D. de Florian, G. Ferrera and M. Grazzini, Eur. Phys. J. C **72** (2012) 2195 [arXiv:1209.0158 [hep-ph]], G. Bozzi, S. Catani, D. de Florian and M. Grazzini, Nucl. Phys. B **737** (2006) 73 [hep-ph/0508068].
- [30] A. Banfi, M. Dasgupta and S. Marzani, Phys. Lett. B **701** (2011) 75 [arXiv:1102.3594 [hep-ph]].
- [31] A. Banfi, M. Dasgupta and R. M. Duran Delgado, JHEP **0912** (2009) 022 [arXiv:0909.5327 [hep-ph]].